ACS OMEGA

http://pubs.acs.org/journal/acsodf

Article

Role of a Nanocomposite Pour Point Depressant on Wax Deposition in Different Flow Patterns from the Perspective of Crystallization Kinetics

Chuanshuo Wang, Hongju Chen, Haitao Shi, Ke Ma, Qianli Ma, and Jing Gong*

Cite This: *ACS Omega* 2022, 7, 11200−11207

Read Online

ACCESS | Metrics & More | Article Recommendations | Supporting Information

ABSTRACT: Wax deposition is one of the core issues affecting flow assurance studies of crude oil pipelines, particularly with deep and ultradeep water conditions. Nanocomposite pour point depressants (NPPDs) provide a novel and effective strategy for inhibiting wax deposition and have recently attracted increasing research attention. Although recent advances have been made in understanding the performance and mechanism of NPPDs, the effect of flow pattern remains an open question. In this paper, deposition thicknesses of waxy oils with different flow patterns and NPPD dosages were obtained using a flow loop experimental device. It was found that the NPPD used in the current work can effectively inhibit the formation of wax deposition layers in different flow patterns. The Avrami model-focused beam reflectance measurement and polarizing microscope experiment method were used to characterize crystallization kinetics parameters and mesoscopic structure parameters of wax crystals. The consistency of results from Avrami equation fitting parameters, wax crystal morphology, and particle number supported the validity of crystallization kinetics analysis. The mechanisms of NPPD in different flow regimes were discussed. The inhibition of laminar and turbulent deposition layers by NPPD was attributed to the improvement of wax crystal morphology and the reduction of wax crystal number, respectively. This has important consequences for our understanding of the utilization and mechanism of nanocomposite pour point depressants.

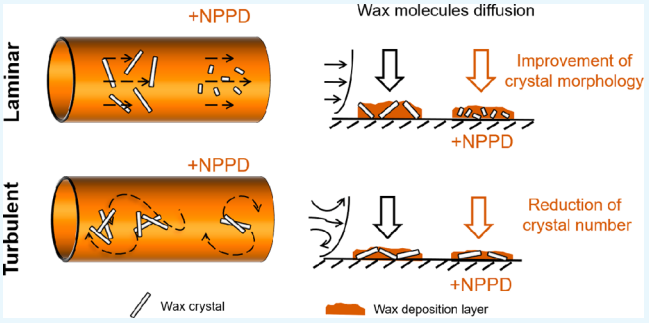

1. INTRODUCTION

Wax deposition poses severe problems for submarine pipeline flow assurance due to the low temperature of the pipe wall and the prevalence of waxy oil.[1] Over the past few decades, substantial effort has been expended in exploring wax mitigation techniques, including hot oiling/water, cold flow, pour point depressants, wax crystal modifiers, and mechanical/biological treatments. Among these treatment techniques, the chemical treatment method has been used for efficient mitigation of wax deposition with lower dosages and lower cost than other techniques.[2]

It is now well-established from a variety of studies that the efficiency of traditional polymer reagents depends primarily on the composition of the waxy oil. To overcome some of the limitations of pour point depressants, many researchers have opted to use nanocomposite methods, commonly known as nanocomposite pour point depressants (NPPDs), in an attempt to improve stability and universality. NPPD is a composite of nanoparticles and polymer molecules, the main fraction of which comprises nanoparticles with small sizes and large specific surface areas. Many studies extend the use of nanoparticles by grafting long polymer chains onto particle surfaces, and this imparts pour point depressants with characteristic mechanical properties of nanomaterials.[3−5] Previous research evaluating viscosities, yield stress, and wax crystal morphologies has established that NPPD is superior to traditional polymer pour point depressants.[6,7] To date, only a limited number of wax deposition processes and mechanisms involving chemical reagents have been identified.

Chi et al.[8] used ethylene vinyl acetate (EVA) copolymer and maleic anhydride copolymer (MAC) and first reported that they effectively reduced the deposition mass but increased the wax content and higher carbon number fraction in the deposit. Yang et al.[9] also investigated the deposition composition using polyoctadecyl acrylate (POA) and confirmed that the wax content, wax appearance temperature, and critical carbon number of the deposition were increased with pour point depressants. Furthermore, Zhu et al.[10] and Ridzuan et al.[11] studied the wax deposition properties of NPPDs under

Received: January 4, 2022
Accepted: March 11, 2022
Published: March 22, 2022

different hydraulic and thermal conditions relevant to the petroleum industry via the Couette or cold finger wax deposition experimental device. The results showed that NPPDs were more effective than traditional polymers in decreasing deposition thickness. Additionally, the detrimental effects of NPPDs caused pigging operation problems with increased wax content. Based on physical property analyses, a preliminary mechanism for wax deposition with NPPD has been proposed. Pour point depressants are capable of improving the morphologies of wax crystals and weakening the initial gel structure. Moreover, they reduce the viscosity of waxy oil and accelerate diffusion of wax molecules. In a pipe flow transporting waxy oil, a deposition layer with a high wax content and hardness tends to form on the pipe wall.[12] While the general physical picture described here was fairly accepted, a detailed understanding of the mechanism of NPPD in different flow patterns remained elusive.

In wax deposition dominated by a molecular diffusion mechanism,[13−15] the role of nucleation and growth by wax crystals has been given sufficient attention in most previous studies of wax deposition.[16−18] Moreover, the exciting prospects of NPPDs have motivated extensive research, which nevertheless has not culminated in a satisfactory understanding of the mechanism for interaction between the NPPD and wax. The nucleation, growth, and crystallization characteristics of wax molecules under the action of NPPD undoubtedly affect the deposition of waxy oil. This paper studies the NPPD deposition performance and mechanism from the perspective of crystallization kinetics. Flow loop wax deposition experiments were designed with varying NPPD concentrations and flow regimes. By employing the qualitative Avrami theory,[19,20] the crystallization/deposition kinetics parameters were illuminated. The total number and morphology of wax crystals were characterized by focusing beam reflectance measurement and polarizing microscopy to support the validity of crystallization kinetics analysis. An improved understanding of the crystallographic level that governs wax deposition formation is essential for utilization and mechanism of nanocomposite pour point depressants.

2. MATERIALS AND METHODS

2.1. Materials. The waxy oil sample consisted of model oil and 7 wt % paraffin. The wax appearance temperature was 25 °C. At 30 °C, the density of waxy oil was 782.5 kg/m^3 and the viscosity was 1.8 mPa·s. The raw materials of waxy model oil used in the experiment were extracted from crude oil. Other characteristics of the waxy oil sample converged to the same points as those in our previous work.[12] The NPPD used in the flow loop was synthesized by melting and blending organically modified nano-montmorillonite and ethylene/vinyl acetate copolymers. The organically modified montmorillonite was obtained by the so-called cation-exchange reaction of sodium montmorillonite clay with hexadecyl trimethylammonium bromide according to the method reported by Qin et al.[19] For more details on synthetic processes and methodologies of the NPPD, we refer the reader to recent articles by He et al.[20] and Gao et al.[21] To ensure the homogeneity of the nanocomposites, NPPD was dissolved in diesel solvent at a concentration of 3 wt %, stirred for 30 min, and then added to the waxy oil. The waxy model oils were preheated to 60 °C for 60 min to eliminate the influence of hot history.

2.2. Methods. *2.2.1. Flow Loop Deposition Experiments.* A flow loop apparatus was used to study wax deposition under a wide range of NPPD dosages, covering both the laminar and turbulent flow regimes, by investigating the growth of deposition thickness as a function of time. The flow loop apparatus was made of a stainless-steel tube with an inner diameter of 20 mm, a wall thickness of 2.5 mm, and a total length of approximately 16 m. It embodied a test section and reference section, centrifugal pump, tank, temperature control system (water bath, ribbon heater), and data acquisition system (Figure 1). Remarkably, there was an injection hole

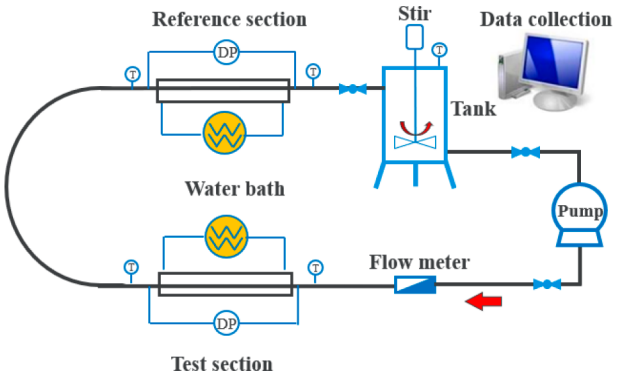

Figure 1. Schematic of the flow loop apparatus.

above the tank, a stirrer (with anchor propeller), and a temperature sensor and a water jacket layer outside the tank. The above accessories were convenient for controlling the additive temperature (55 °C) and the stirring rate (200 rpm) and ensuring uniform dispersion of NPPD in the experimental fluid. We varied the NPPD dosage from 0 to 200 at intervals of 50 mg/kg. The differential pressure of the pipe sections with varying NPPD dosages and deposition time was recorded during these experiments (Supporting Information S1). Based on the pressure drop method,[22] the average thickness of the deposition layer was calculated and analyzed at different flow regimes and NPPD concentrations.

Flow rates were fixed at 3.0 and 6.0 kg/min, which yielded laminar (Re = 1769) and turbulent (Re = 3538) flow patterns to simulate flow regimes for industrial-scale field pipelines transporting waxy crude oils. Additionally, the oil temperature was 30 °C (the wax appearance temperature was 25 °C), and the coolant temperature for each case was adjusted to maintain the initial inner wall temperature at 10 °C. A temperature difference of 20 °C provided the thermodynamics for wax deposition. The wax deposition's duration was set to 8 h.

2.2.2. Avrami Equation Theoretical Analysis. It is generally thought that, of the mechanisms proposed for wax deposition in pipelines, molecular diffusion makes dominant contributions to deposition formation and is accompanied by nucleation and crystallization processes.[13]

Yang et al.[16] demonstrated through a series of deposition experiments that a single molecular diffusion mechanism was insufficient to describe the wax deposition process, and nucleation, growth, and aggregation of wax crystals near the pipe wall were important components that cannot be ignored. With the aid of a visualization window, Cabanillas et al.[17] observed that the transport velocity of wax crystals or aggregates flowing in suspension gradually slowed as they approached and joined the wax deposition layer. Subsequently, Haj-Shafiei et al.[18] proposed a new method for in situ characterization of wax crystal structures and crystallization

https://doi.org/10.1021/acsomega.2c00068
ACS Omega 2022, 7, 11200−11207

kinetics parameters based on laser scanning confocal microscopy, which provided new ideas for an in-depth understanding of the relationship between wax crystallization kinetics and solid-phase deposition. Ismail et al.[23] studied the crystallization kinetics and deposition mechanism under oscillating conditions according to Avrami theory.

The Avrami equation is a well-known principle used to gain insights into crystallization kinetics. It has been used in the past to investigate the mechanical properties of paraffin wax deposition.[24,25] Continuing efforts have been dedicated to deducing and simplifying Avrami's original equation,[23] especially for applications in bulk crystallization. For paraffin wax deposition, the Avrami equation can be written as

$$\log[-\ln(1-\delta_r)] = \log K + n\log(t) \quad (1)$$

where δ_r is the normalized deposition mass and t is the deposition time (min). By plotting $\log[-\ln(1-\delta_r)]$ versus $\log(t)$ and fitting the data with the linear least-squares method, the slope of the straight-line n and the intersection $\log K$, which is related to the crystal morphology and quantity, can be extracted.[25,26] δ_r in eq 1 is the ratio of deposition mass at time t to the maximum deposition mass. This calculation was used to further evaluate crystallization/deposition kinetics with NPPDs and is presented in Supporting Information S2, where data for deposition thickness and the wax deposition calculation method can also be found.

2.2.3. Characterization of Wax Crystal Size, Number, and Morphology. Characterization was completed by focused beam reflectance measurement (FBRM) (METTLER TOLEDO, Switzerland), which allowed the chord length and total counts of wax crystals at various flow patterns and NPPD dosages to be obtained. The unique feature about this process was that the test sample section was equipped with a circulating water bath and an agitator so that the cooling process and Reynold number could be controlled concurrently, as shown in Figure 2.

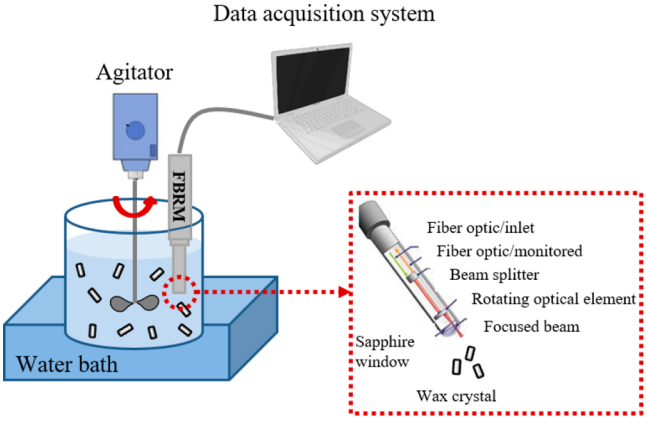

Figure 2. Schematic diagram of the FBRM measurement.

An equally spaced axial four-blade propeller was used to stir the waxy oil sample. The impeller entered the liquid at a 0° angle from the top and was centered with a clearance from the bottom equal to the impeller diameter. The stirring speed was controlled by an agitator (IKA, Germany) with built-in tachometer control. To monitor the wax crystal size and distribution at different flow regimes and NPPD dosages, the impeller Reynolds number and the flow loop Reynolds number were set to the same value. Stirring speeds of 36 and 63 rpm correspond to laminar and turbulent flow in the flow loop, respectively. The calculation formula is shown below.

$$N = \frac{\mu \mathrm{Re}}{(\rho d^2)} \quad (2)$$

In eq 2, μ is the liquid dynamic viscosity, ρ is the density, and d is the impeller diameter. Stirring of the waxy oil sample was started 5 min before the NPPD was added to achieve uniform mixing. During the FBRM test, the oil sample was cooled from 30 to 10 °C. The cooling rate was maintained constant at 0.5 °C/min via the same pump speed of the water bath (F25 Julabo, Germany). The number and distribution of crystals were repeated after the constant temperature of 10 °C for 10 min. The oil sample was replaced and the measurement repeated. The following results were the average of the repeated test results. At the same time, we dipped the oil sample in the FBRM experimental beaker with a dropper and dropped it on the slide. A polarizing microscope (BX51, OLYMPUS) with a 20× magnification objective lens was used to observe the morphology of waxy crystals. Sampling and observation were repeated (at least three times).

3. RESULTS AND DISCUSSION

3.1. Wax Deposition Thickness in Two Flow Patterns. To investigate the characteristics of the NPPD in the pipeline flow, flow loop experiments were carried out with two flow patterns to fill the gaps in our understanding. The evolution of deposition thickness with different flow patterns and NPPD dosages is shown in Figure 3.

First, the clear trend for decreasing wax deposition thickness with increasing NPPD dosage suggested that NPPDs effectively inhibit wax deposition under different flow patterns. For instance, at 8 h, the deposition thickness in the laminar flow had decreased from 7.01 (0 mg/kg) to 4.10 mm (200 mg/kg). Wax deposition thickness at 8 h decreased from 3.90 to 2.34 mm for turbulent flow. The reduction rate of laminar and turbulent wax deposition thickness was 41.5 and 40%, respectively. Second, Figure 3 reveals that there was a steady decline in deposition thickness with increasing flow rate. The 8 h deposition thickness with laminar flow was in the range of 4.10−7.01 mm, and this was thicker than the range for turbulent flow (2.34−3.90 mm). These observations were consistent with previous studies showing that chemical agents and flow regulation served to arrest the formation of wax deposits in field operations.[27,28] Further analyses of deposition characteristics based on crystallization kinetics are given in the next section.

3.2. Crystallization/Deposition Kinetics Analyses. Analysis of the fitting values (n, K) for the Avrami equation allowed us to obtain crystallization kinetics parameters for the waxy oil sample as a function of flow patterns and NPPD dosages. The Avrami plots for different flow patterns are shown in Figure 4.

From the preceding summary of Avrami plots, it should be evident that good linear relationships were seen for all of these cases, indicating the validity of the Avrami method. The fitted coefficients of determination (R^2) for different flow regimes and NPPD dosages were greater than 0.94. The slope (n) and intercept ($\log K$) of Avrami plots referred to as the phenomenological index of crystallization was extracted from Figure 4 and is summarized in Table 1.

https://doi.org/10.1021/acsomega.2c00068
ACS Omega 2022, 7, 11200−11207

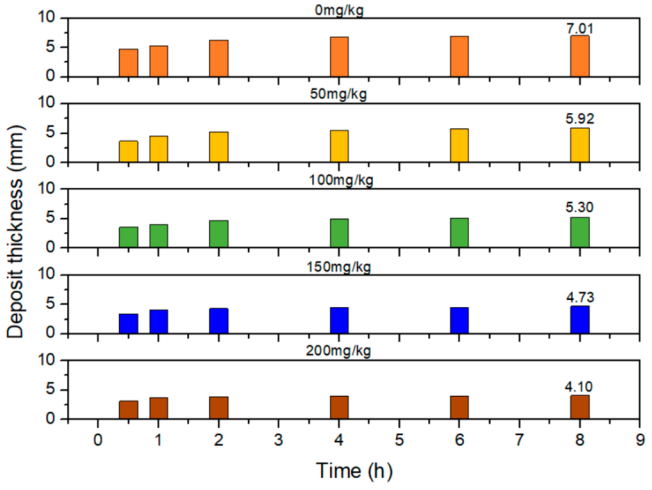

(a) Laminar flow

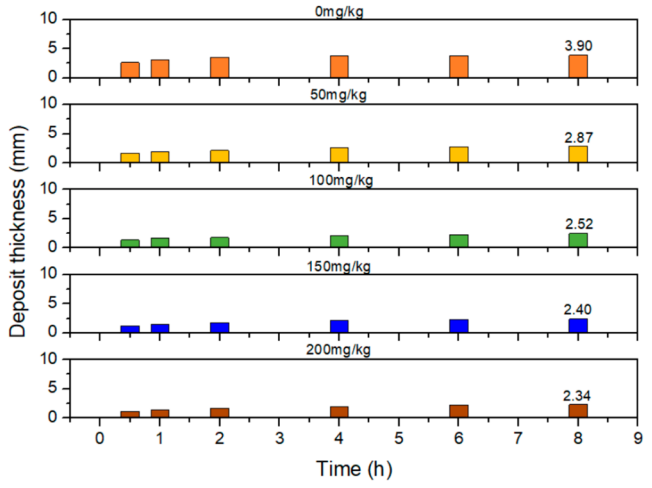

(b) Turbulent flow

Figure 3. Deposition thickness for two flow patterns.

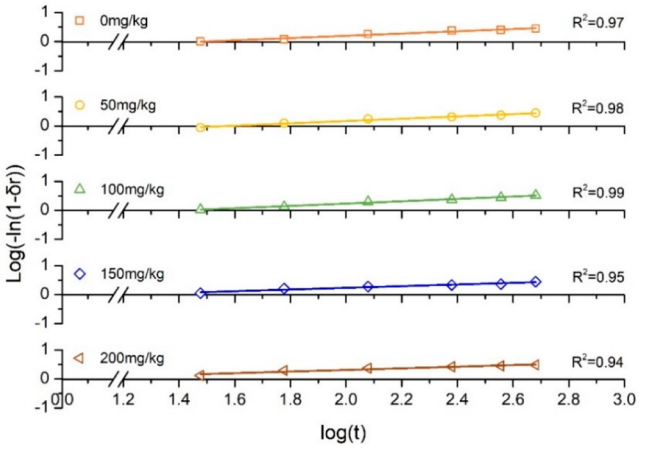

(a) Laminar flow

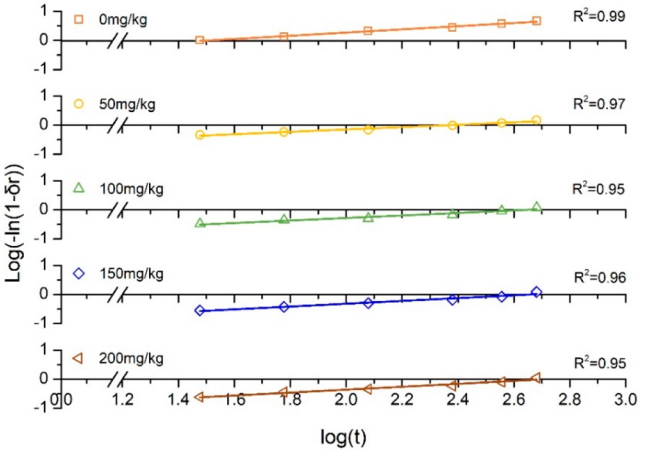

(b) Turbulent flow

Figure 4. Avrami fitting diagram for different flow patterns.

The Avrami exponent n is related to the morphological structures of crystals and their crystalline nucleation process.[19] In general, for polymeric and organic systems, the Avrami exponents are 1, 2, and 3 for rod, disc, and spherical crystals, respectively. The Avrami exponent for secondary nucleation is equal to the primary nucleation index plus 1.[29] Primary nucleation is spontaneous nucleation that occurs in supersaturated solutions without the presence of crystals and includes homogeneous and heterogeneous nucleation.[30] Homogeneous nucleation arises in pure intrinsic solutions, whereas heterogeneous nucleation occurs due to induction by foreign solid surfaces such as impurities or particles in solution.[31,32] The waxy oil system used with NPPD in this study is assigned to the heterogeneous nucleation category.

Other factors, such as the crystal growth mechanism and temperature, also significantly affect the Avrami exponent. Siyal et al.[33] studied the crystallization kinetics of fly ash geopolymers at different temperatures and mineral ratios and found n values ranging from 0.0931 to 0.2321. A smaller Avrami exponent ($n < 0.5$) is the reason for one-dimensional diffusion growth of a crystal. In our experiment, fitted Avrami exponents for different flow rates and NPPD concentrations were also less than 0.5, indicating that the mechanism for wax crystal growth was similar to those of geopolymers. The needle-like wax crystal morphology (Figure 7) provided evidence to support this viewpoint.[12,34]

Table 1. Summary of n and K Values in the Fitting Results of the Avrami Equation

	laminar		turbulent	
NPPD dosage	n	K	n	K
0 mg/kg	0.40	0.25	0.45	0.24
50 mg/kg	0.28	0.26	0.41	0.18
100 mg/kg	0.21	0.32	0.38	0.16
150 mg/kg	0.16	0.36	0.39	0.13
200 mg/kg	0.11	0.38	0.41	0.12

Table 1 and Figure 5 showed that the NPPD-doped oil exhibited an n value significantly lower than that of the undoped oil. This suggested that the wax crystalline morphology was improved by the NPPD.[35] Continuous improvement in wax crystal morphology was indicated by a decrease in n in the laminar flow. However, the n value for turbulent flow did not decrease significantly with increasing NPPD dosage, and there were fluctuating trends. This implied that irregular motion of fluid particles in the turbulent flow state changed the mechanisms for the role of NPPD. The improvement of wax crystal morphology was not the major factor inhibiting wax deposition in the turbulent flow.

https://doi.org/10.1021/acsomega.2c00068
ACS Omega 2022, 7, 11200−11207

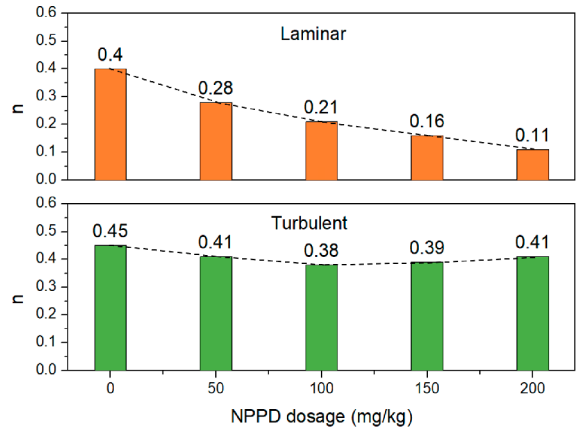

Figure 5. Changes in n as a function of NPPD dosage.

Table 1 and Figure 6 compared the results for K obtained from the intersections of Avrami plots. What stands out in Figure 6 was that there were significant differences for the two flow pattern conditions. The crystallization kinetics parameter K increased gradually in the laminar flow as more NPPD was dissolved in the waxy oil, but the K in the turbulent flow was inversely related to NPPD concentrations within the NPPD concentration range of 0−200 mg/kg. In $K = gNv^n$, g and N are the geometrical factor and number of wax crystals, respectively, v is the growth rate, and n is the Avrami exponent.[36] K is mainly related to the number of crystals, geometry, and growth rate. It is noteworthy that both the geometrical factor g and Avrami exponent n decreased under laminar flow because of the improvement of the wax crystal morphology. The increase in K value was mainly related to the number of wax crystals, which increased as a function of NPPD dosage. However, the wax crystal morphology and Avrami exponent n did not change significantly in the turbulent flow. The decrease in K value was mainly attributed to the decrease in the number of wax crystals.

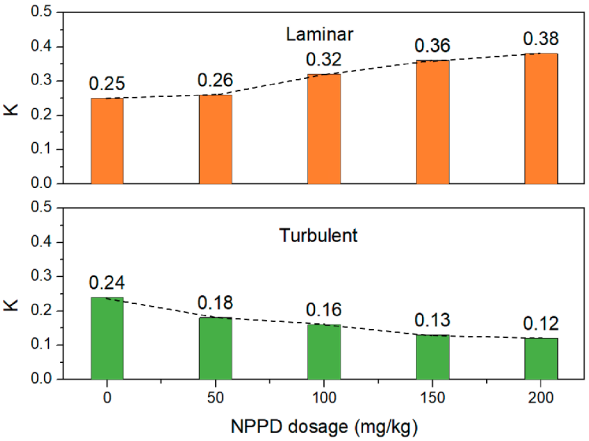

Figure 6. Changes in K as a function of NPPD dosage.

3.3. Wax Crystal Morphology, Particle Number, and Particle Size. To provide more convincing evidence, a systematic study of the morphology of wax crystals in the laminar and turbulent flows was performed with polarizing microscope images, as presented in Figure 7.

We note that, as expected, the wax crystals with the addition of NPPD became smaller as compared with that of undoped oil in the laminar flow. The original high aspect ratio wax crystals were replaced by fine rice-like wax crystals with NPPD (Figure 7b), which was consistent with our previous observations[12] showing that the NPPD can effectively improve wax crystal morphology. The experimental data presented in Figure 7c,d were, seemingly, the first published results that displayed the spatial variation of the wax crystal morphology under turbulent flowing conditions. The needle-like crystals tended to aggregate under turbulent flow, forming wax crystal clusters (Figure 7c). Moreover, the morphology of the wax crystal clusters was not significantly altered by NPPD. The obvious thing was that the number of clusters decreased, and the clusters became brighter after the addition of NPPD. It meant that the needle-like wax crystals within the aggregates were arranged more densely (Figure 7d). The irregular motion of fluid particles promoted crystal aggregation and entanglement.[37] Wax crystals in the turbulent flow tended to gather more than those in the laminar flow, especially for the case of adding NPPD.

To further analyze the discrepancy of wax crystals resulting from different dosages of NPPD in two flow patterns, we conducted several groups of FBRM tests by monitoring the size distribution and the total number of wax crystals.

Figure 8 reveals the effect of concentration of NPPD on wax crystal size distribution. Under the laminar flow, the number of wax crystals with small particle size (<32 μm) increased with increasing NPPD dosage, whereas the number of wax crystals with large particle size (>32 μm) decreased. Accompanied by an increase in NPPD dosage, the size of the wax crystals was smaller than that of undoped oil. These results underscored the improvement of wax crystal morphology by NPPD. However, under the turbulent flow, the crystal's size distributions fluctuated with increasing NPPD dosage. Similar trends can be observed for the Avrami exponent n (Figure 5).

The total number of wax crystals as a function of NPPD dosage in two flow patterns is shown in Table 2. As NPPD dosage increased, there was a tendency to form more waxy crystals in the laminar flow. However, the trend of the total particle number in the turbulent flow exhibited the opposite trend, in which it decreased as the NPPD dosage increased. These results were consistent with the trend for K from fitting of the Avrami equation (Figure 6).

3.4. Discussion of the Role of a Nanocomposite Pour Point Depressant on Wax Deposition. These results and the analysis of crystallization kinetics promote discussions of the mechanisms for interactions between NPPD and wax deposition impacted by flow patterns (Figure 9). In the pipe flow environment, fluid particles move in a parallel fashion along the direction of oil flow and do not mix in the laminar flow, so the structures of wax crystals are relatively less disturbed by the external fluid. The main role of the NPPD in heterogeneous nucleation consists of serving as templates promoting wax nucleation and therefore leading to a slight increase in the total number of wax crystals (Table 2). At the same time, the polymer in the NPPD significantly improves the morphology of wax crystals through cocrystallization and adsorption mechanisms.[38−40] The results for the Avrami exponent n (Figure 5) and wax crystal size distribution (Figure 8a) support this argument. The improvement of crystal morphology plays a pivotal role in the wax deposition inhibition by NPPD under laminar flow. The improved crystal morphology (reduction of wax crystal size) leads to a weakening of its ability to encapsulate oil in the network, thus inhibiting the deposition layer. In the turbulent flow,

https://doi.org/10.1021/acsomega.2c00068
ACS Omega 2022, 7, 11200−11207

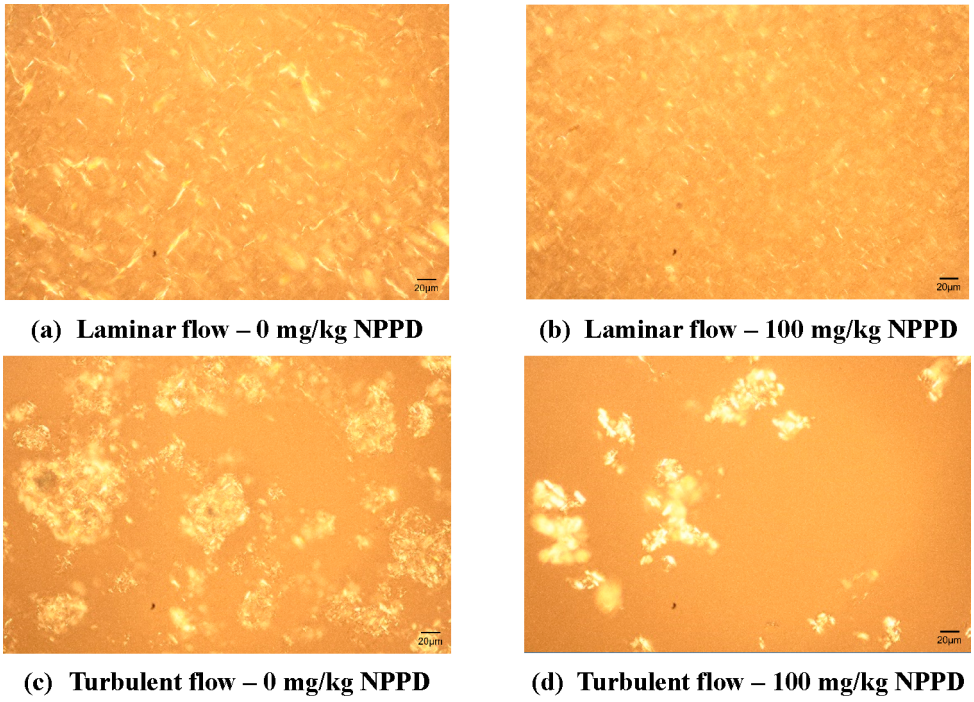

Figure 7. Wax crystal morphology of undoped oil and doped oil under different flow patterns.

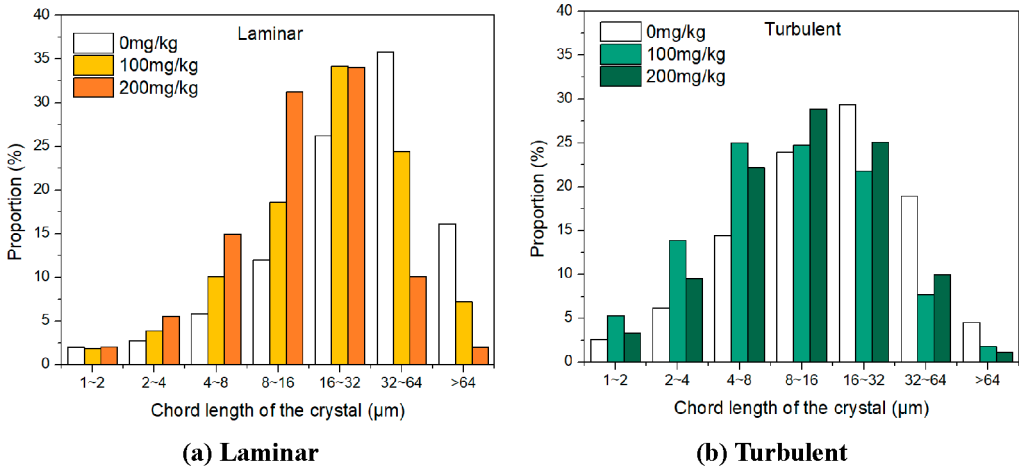

Figure 8. Wax crystals size distribution in two flow patterns.

Table 2. Numbers of Wax Crystals in Two Flow Patterns

NPPD dosage	laminar	turbulent
0 mg/kg	16705	22367
50 mg/kg	17434	18943
100 mg/kg	17935	16141
150 mg/kg	18202	12953
200 mg/kg	18778	9241

irregular motion of fluid particles interferes with the interaction between wax and NPPD. Polymer disentanglement caused by flow disturbances[41] could change the mechanisms for the role of the NPPD. The disentangled polymer side chains and main chain further promote cocrystallization and adsorption interactions, thereby inhibiting the nucleation and growth of wax crystals and reducing their number, as shown in Table 2. The improvement of crystal morphology by NPPD in the turbulent flow is negligible compared to that in the laminar flow. The reduction of crystal number is the main mechanism for the inhibition of wax deposition under turbulent flow.

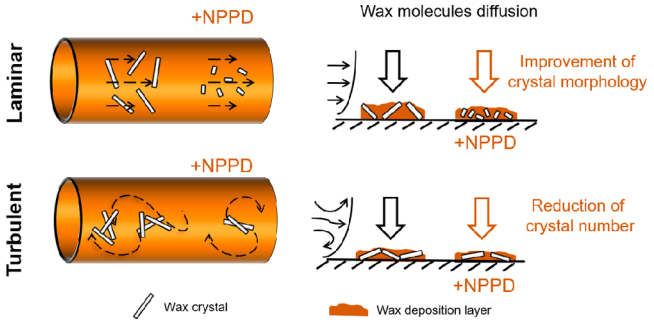

Figure 9. Schematic of the wax deposition mechanism of NPPD in different flow patterns.

https://doi.org/10.1021/acsomega.2c00068
ACS Omega 2022, 7, 11200−11207

4. CONCLUSIONS

This study was designed to investigate the performance of wax deposition in different flow patterns after the addition of NPPD.

It was found that the NPPD used in the current work can effectively inhibit the formation of wax deposition layers in different flow patterns. The wax deposition thickness with 200 mg/kg NPPD in the laminar flow and the turbulent flow can be reduced by 41.5 and 40%. The wax deposition mechanism of NPPD in different flow patterns from the perspective of crystallization kinetics was further discussed.

Continuous improvement of wax crystal morphology is indicated by the decrease of the Avrami exponent n with increasing NPPD dosage in the laminar flow regime. Experimental results from the characterization of wax crystal size and morphology verified again that the addition of NPPD improved the wax crystal morphology, from high aspect ratio crystals to fine rice-like crystals. Based on these, it was inferred that the inhibition of NPPD on the laminar flow deposition layer was mainly due to the improvement of wax crystal morphology.

The crystallization kinetics parameter K decreased gradually in the turbulent flow as more NPPD was dissolved in the waxy oil, consistent with the downward trend in total particle number under turbulent flow as NPPD dosage increased. However, the variation tendency of the Avrami exponent n and wax crystal size fluctuated, and no significant difference in the wax crystal morphology can be observed with increasing NPPD dosage. The results of the analysis provided information regarding the inhibition of NPPD on turbulent flow deposition by the reduction of crystal number rather than by the improvement of wax crystal morphology.

■ ASSOCIATED CONTENT

Supporting Information

The Supporting Information is available free of charge at https://pubs.acs.org/doi/10.1021/acsomega.2c00068.

Relevant flow loop experimental data including the original differential pressure and deposition thickness data (S1); relevant wax deposition thickness calculation method: Darcy−Weisbach formula (S2) (PDF)

■ AUTHOR INFORMATION

Corresponding Author

Jing Gong − *National Engineering Laboratory for Pipeline Safety/MOE Key Laboratory of Petroleum Engineering/Beijing Key Laboratory of Urban Oil and Gas Distribution Technology, China University of Petroleum, Beijing 102249, P.R. China;* orcid.org/0000-0002-4771-7119; Email: ydgj@cup.edu.cn

Authors

Chuanshuo Wang − *National Engineering Laboratory for Pipeline Safety/MOE Key Laboratory of Petroleum Engineering/Beijing Key Laboratory of Urban Oil and Gas Distribution Technology, China University of Petroleum, Beijing 102249, P.R. China*

Hongju Chen − *China National Offshore Oil Cooperation Research Center, Beijing 100027, P.R. China*

Haitao Shi − *National Engineering Laboratory for Pipeline Safety/MOE Key Laboratory of Petroleum Engineering/Beijing Key Laboratory of Urban Oil and Gas Distribution Technology, China University of Petroleum, Beijing 102249, P.R. China*

Ke Ma − *National Engineering Laboratory for Pipeline Safety/MOE Key Laboratory of Petroleum Engineering/Beijing Key Laboratory of Urban Oil and Gas Distribution Technology, China University of Petroleum, Beijing 102249, P.R. China*

Qianli Ma − *Jiangsu Key Laboratory of Oil and Gas Storage and Transportation Technology, Changzhou University, Changzhou 213164, P.R. China;* orcid.org/0000-0002-2679-617X

Complete contact information is available at: https://pubs.acs.org/10.1021/acsomega.2c00068

Notes

The authors declare no competing financial interest.

■ ACKNOWLEDGMENTS

The authors thank the National Natural Science Foundation of China (51774303, 51534007), the National Science & Technology Specific Project (2016ZX05028-004-001), and Science Foundation of China University of Petroleum, Beijing (C201602) for providing support for this work.

■ REFERENCES

(1) Singh, P.; Venkatesan, R.; Fogler, H. S.; Nagarajan, N. Morphological evolution of thick wax depositions during aging. *AIChE J.* **2001**, *47*, 6.

(2) Chi, Y.; Yang, J.; Sarica, C.; Daraboina, N. A Critical Review of Controlling Paraffin Deposition in Production Lines using Chemicals. *Energy Fuels.* **2019**, *33*, 2797−2809.

(3) Norrman, J.; Solberg, A.; Sjöblom, J.; Paso, K. Nanoparticles for waxy crudes: effect of polymer coverage and the effect on wax crystallization. *Energy Fuels.* **2016**, *30*, 5108−5114.

(4) Al-Sabagh, A. M.; Betiha, M. A.; Osman, D. I.; Hashim, A. I.; El-Sukkary, M. M.; Mahmoud, T. Preparation and evaluation of polymethyl methacrylate-graphene oxide nano-hybrid polymers as pour point depressants and flow improvers for waxy crude oil. *Energy Fuels.* **2016**, *30*, 7610−7621.

(5) Sharma, R.; Mahto, V.; Vuthaluru, H. Synthesis of PMMA/modified graphene oxide nanocomposite pour point depressant and its effect on the flow properties of Indian waxy crude oil. *Fuel.* **2019**, *235*, 1245−1259.

(6) Yang, F.; Paso, K.; Norrman, J.; Li, C.; Oschmann, H.; Sjoblom, J. Hydrophilic nanoparticles facilitate wax inhibition. *Energy Fuels.* **2015**, *29*, 1368−1374.

(7) Huang, H.; Wang, W.; Peng, Z.; Li, K.; Gan, D.; Zhang, S.; Ding, Y.; Wu, H.; Gong, J. The effect of cooling processes on the yield stress of waxy model oil with nanocomposite pour point depressant. *J. Pet. Sci. Eng.* **2019**, *175*, 828−837.

(8) Chi, Y.; Daraboina, N.; Sarica, C. Investigation of inhibitors efficacy in wax deposition mitigation using a laboratory-scale flow loop. *AIChE J.* **2016**, *62*, 4131−4139.

(9) Yang, F.; Cheng, L.; Liu, H.; Yao, B.; Li, C.; Sun, G.; Zhao, Y. Comb-like Polyoctadecyl Acrylate (POA) Wax Inhibitor Triggers the Formation of Heterogeneous Waxy Oil Gel Deposits in a Cylindrical Couette Device. *Energy Fuels.* **2018**, *32*, 373−383.

(10) Zhu, H.; Li, C.; Xiu, Z.; Zhao, Z.; Mu, K.; Dai, H.; Wang, F.; Yang, F.; Yao, B. Effect of Ethylene-Vinyl Acetate Copolymer/Amino-Functionalized Polymethylsilsesquioxane Composite Wax Inhibitor on the Rheological and Wax Depositing Characteristics of Waxy Crude Oil. *Energy Fuels.* **2020**, *34*, 8120−8128.

(11) Ridzuan, N.; Subramanie, P.; Uyop, M. F. Effect of pour point depressant (PPD) and the nanoparticles on the wax deposition, viscosity and shear stress for Malaysian crude oil. *Pet. Sci. Technol.* **2020**, *38*, 929−935.

(12) Wang, C.; Zhang, M.; Wang, W.; Ma, Q.; Zhang, S.; Huang, H.; Peng, Z.; Yao, H.; Li, Q.; Ding, Y.; Gong, J. Experimental Study of the Effects of a Nanocomposite Pour Point Depressant on Wax Deposition. *Energy Fuels.* **2020**, *34*, 12239−12246.
(13) Singh, P.; Venkatesan, R.; Fogler, H. S.; Nagarajan, N. Formation and aging of incipient thin film wax-oil gels. *AIChE J.* **2000**, *46*, 1059−1074.
(14) Zheng, S.; Khrutphisit, T.; Fogler, H. S. Entrapment of Water Droplets in Wax Depositions from Water-in-Oil Dispersion and Its Impact on Deposition Build-up. *Energy Fuels.* **2017**, *31*, 340−350.
(15) Zheng, S.; Fogler, H. S. Fundamental investigation of wax diffusion characteristics in water-in-oil emulsion. *Ind. Eng. Chem. Res.* **2015**, *54*, 4420−4428.
(16) Yang, J.; Lu, Y.; Daraboina, N.; Sarica, C. Wax deposition mechanisms: Is the current description sufficient? *Fuel.* **2020**, *275*, 117937.
(17) Cabanillas, J. P.; Leiroz, A. T.; Azevedo, L. F. A. Wax Deposition in the Presence of Suspended Crystals. *Energy Fuels.* **2016**, *30*, 1−11.
(18) Haj-Shafiei, S.; Workman, B.; Trifkovic, M.; Mehrotra, A. K. In-Situ Monitoring of Paraffin Wax Crystal Formation and Growth. *Cryst. Growth Des.* **2019**, *19*, 2830−2837.
(19) Qin, H. L.; Zhang, S. M.; Liu, H. J.; Xie, S. B.; Yang, M. S.; Shen, D. Y. Photo-oxidative degradation of polypropylene/montmorillonite nanocomposites. *Polymer.* **2005**, *46*, 3149−3156.
(20) He, C.; Ding, Y.; Chen, J.; Wang, F.; Gao, C.; Zhang, S.; Yang, M. Influence of the nano-hybrid pour point depressant on flow properties of waxy crude oil. *Fuel.* **2016**, *167*, 40−48.
(21) Gao, C.; He, C.; Ding, Y.; Chen, J.; Wang, F.; Liu, P.; Zhang, S.; Li, Z.; Yang, M. The yield stress of model waxy oil after incorporation of organic montmorillonite. *Fuel.* **2017**, *203*, 570−578.
(22) Chen, X. T.; Butler, T.; Volk, M.; Brill, J. Techniques for Measuring Wax Thickness During Single and Multiphase Flow. SPE-38773-MS. In *Proceedings of Society of Petroleum Engineers Technical Conference and Exhibition*; San Antonio, Texas, 1997.
(23) Ismail, L.; Westacott, R. E.; Ni, X. On the effect of wax content on paraffin wax deposition in a batch oscillatory baffled tube apparatus. *Chem. Eng. J.* **2008**, *137*, 205−213.
(24) Avrami, M. Kinetics of Phase Change. I General Theory. *J. Chem. Phys.* **1939**, *7*, 1103−1112.
(25) Avrami, M. Kinetics of Phase Change. II Transformation-Time Relations for Random Distribution of Nuclei. *J. Chem. Phys.* **1940**, *8*, 212−224.
(26) Hosseinipour, A.; Japper-Jaafar, A.; Yusup, S.; Ismail, L. Application of the Avrami theory for wax crystallisation of synthetic crude oil. *Int. J. Eng., Trans. A* **2019**, *32*, 18−27.
(27) Mahir, L. H. A.; Lee, J.; Fogler, H. S.; Larson, R. G. An experimentally validated heat and mass transfer model for wax deposition from flowing oil onto a cold surface. *AIChE J.* **2021**, *67*, 17063.
(28) White, M.; Pierce, K.; Acharya, T. A Review of Wax-Formation/Mitigation Technologies in the Petroleum Industry. *SPE Prod. Oper.* **2018**, *33*, 476−485.
(29) Hay, J. N. Application of the modified avrami equations to polymer crystallisation kinetics. *Polym. Int.* **1971**, *3*, 74−82.
(30) Miller, S. M.; Rawlings, J. B. Model identification and control strategies for batch cooling crystallizers. *AIChE J.* **1994**, *40*, 1312−1327.
(31) Leubner, I. H. Particle nucleation and growth models. *Curr. Opin. Colloid Interface Sci.* **2000**, *5*, 151−159.
(32) Xu, S.; Hou, Z.; Chuai, X.; Wang, Y. Overview of Secondary Nucleation: From Fundamentals to Application. *Ind. Eng. Chem. Res.* **2020**, *59*, 18335−18356.
(33) Siyal, A. A.; Azizli, K. A.; Man, Z.; Ismail, L.; Khan, M. I. Geopolymerization kinetics of fly ash based geopolymers using JMAK model. *Ceram. Int.* **2016**, *42*, 15575−15584.
(34) Huang, H. R.; Wang, W.; Peng, Z.; et al. Magnetic Organic−Inorganic Nanohybrid for Efficient Modification of Paraffin Hydrocarbon Crystallization in Model Oil. *Langmuir.* **2020**, *36*, 591−599.
(35) Huang, H.-R.; Wang, W.; Peng, Z.-H.; Li, K.; Ding, Y.-F.; Yu, W.-J.; Gan, D.-Y.; Wang, C.-S.; Xue, Y.-H.; Gong, J. Synergistic effect of magnetic field and nanocomposite pour point depressant on the yield stress of waxy model oil. *Pet. Sci.* **2020**, *17*, 838−848.
(36) Cheng, S. Z. D.; Wunderlich, B. Modification of the Avrami treatment of crystallization to account for nucleus and interface. *Macromolecules.* **1988**, *21*, 3327−3328.
(37) Venkatesan, R.; Nagarajan, N. R.; Paso, K.; Yi, Y. B.; Sastry, A. M.; Fogler, H. S. The strength of paraffin gels formed under static and flow conditions. *Chem. Eng. Sci.* **2005**, *60*, 3587−3598.
(38) Holder, G. A.; Winkler, J. Crystal-growth poisoning of n-paraffin wax by polymeric additives and its relevance to polymer crystallization mechanisms. *Nature.* **1965**, *207*, 719−721.
(39) Guo, X.; Pethica, B. A.; Huang, J. S.; Prud'Homme, R. K. Crystallization of long-chain n-paraffinsfrom solutions and melts as observed by differential scanning calorimetry. *Macromolecules.* **2004**, *37*, 5638−5645.
(40) Binks, B. P.; Fletcher, P. D. I.; Roberts, N. A.; Dunkerley, J.; Greenfield, H.; Mastrangelo, A.; Trickett, K. How polymer additives reduce the pour point of hydrocarbon solvents containing wax crystals. *Phys. Chem. Chem. Phys.* **2015**, *17*, 4107−4117.
(41) Sun, J.-K.; Sobolev, Y. I.; Zhang, W.; Zhuang, Q.; Grzybowski, B. A. Enhancing crystal growth using polyelectrolyte solutions and shear flow. *Nature.* **2020**, *579*, 73−79.

https://doi.org/10.1021/acsomega.2c00068
ACS Omega 2022, 7, 11200−11207